Comparative Study of PI and Fuzzy Logic Based Speed Controllers of an EV with Four In-Wheel Induction Motors Drive

Submitted: 26th October 2018; accepted: 15th November 2018

Abdelkader Ghezouani, Brahim Gasbaoui, Nouria Nair, Othmane Abdelkhalek, Jemal Ghouili

DOI: 10.14313/JAMRIS_3-2018/17

Abstract:
This paper presents the modeling, control and simulation of an electric vehicle with four in-wheel 15 kw induction motors drive 4WDEV controlled by a direct torque control DTC strategy, where two control techniques are presented and compared for controlling the electric vehicle speed: the first one is based on a classical PI controller while the second one is based on a fuzzy logic controller (FLC). The aim is to evaluate the impact of the proposed FLC controller on the efficiency of the 4WDEV taking into account vehicle dynamics performances, autonomy and battery power consumption. When the classical controller can't ensure the electric vehicle stability in several road topology situations. To show the efficiency of the proposed new control technique on the traction system by 4WDEV. The vehicle has been tested in different road constraints: straight road, sloping road and curved road to the right and left using the Matlab / Simulink environment. The analysis and comparison of the simulation results of FLC and PI controllers clearly show that the FLC ensures better performances and gives a good response without overshoot, zero steady state error and high load robustness rejection, compared to the PI controller which is present an overshoot equal 7.3980% and a rise time quite important (0.2157 s with PI controller and 0.1153 s with FLC). As well as the vehicle range has been increased by about 10.82 m throughout the driving cycle and that the energy consumption of the battery has been reduced by about 1.17% with FLC.

Keywords: *electric vehicle, induction motor, PI controller, fuzzy logic controller FLC, direct torque control DTC, four in-wheel induction motors*

1. Introduction

In electric traction systems, the overall performance of an electric vehicle depends mainly on the type of drive motor used (as an indispensable part of the traction drive) for a four-wheel drive electric vehicle (EV4WD). Among the different types of engines exist in the literature; the induction motor seems to be the candidate that feels better the main characteristics of the propulsion [1], [2]. Due to their good performance (low purchase cost, simple construction, robust, does no. need maintenance, they support overloads prove to go up to 5 or 7 times the nominal torque [3], [4], the good dynamic performance of the torque control). However, these advantages have long been inhibited by the complexity of the control. This complexity is mainly due to the following reasons:

- The analytical model of the induction machine is non-linear.
- Presence of parametric uncertainties and the need to take into account their variation over time. From this fact, various control techniques have been developed to give the induction motor with precision, flexibility of control and the quality of electromagnetic conversion. Direct torque control (DTC) is one of the most popular control techniques for induction motors [5], [6]. This technique is proposed by I. Takahashi and T. Noguchi [7] and Depebrock [8] in the late 1980s. The main advantages of this method are the very fast torque response to load torque changes, less dependencies to machine parameters and a simple control scheme [5], control without modulation of the width of the impulse (MLI), control of flux without using controllers of currents, control without speed sensor is possible since the method does no need accurate information on the rotor position angle [9].

In this article, a new method of speed control based on fuzzy logic controller is proposed for an electric vehicle with four in-wheels induction motor. Compared to a classical PI controller, the proposed approach has the advantages of simplicity, flexibility, and high accuracy. Modelling and simulation are carried out using the Matlab/Simulink tool to investigate the performance of the proposed system. The paper structure is organized as follows: the main components of the proposed pull chain are shown without section 2. Section 3 presents the DTC control strategy of induction motor, the mathematical model of 4WD electric vehicle and electronic differential; as well the design of the PI and FLC speed controllers is show in section 4. Regarding section 5, it shows the simulation results. In the end, section 6 conclusions.

2. 4WD Electric Vehicle Description

The traction chain of the four-wheel drive electric vehicle 4WDEV is shown in Fig. 1. The power structure in this traction chain is composed of four in-wheel induction motors which are supplied by four three-phase inverters. The lithium-ion battery (Lithium-ion) is the main source of the vehicle. It is coupled to a DC-DC bidirectional power bus (Buck-Boost

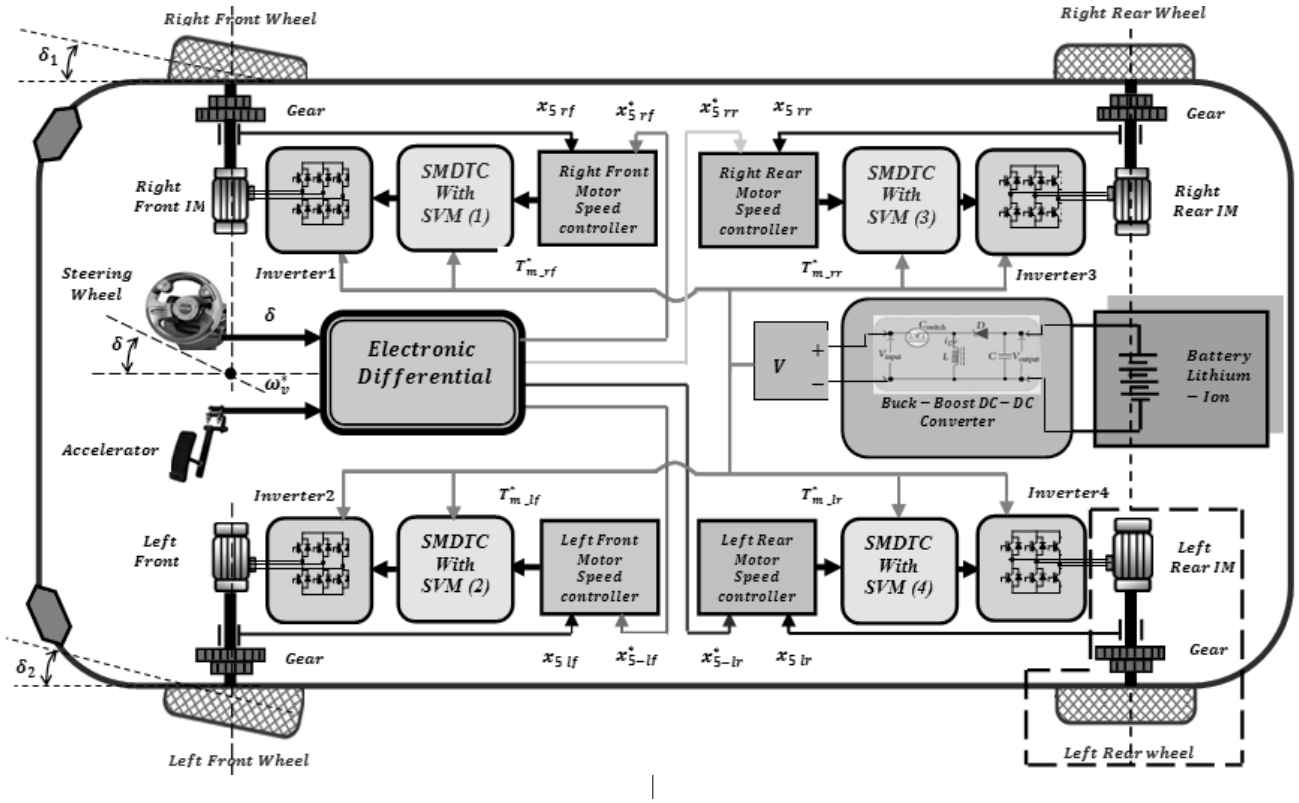

Fig. 1. Electric vehicle with four in-wheels drives 4WD EV schematic diagram

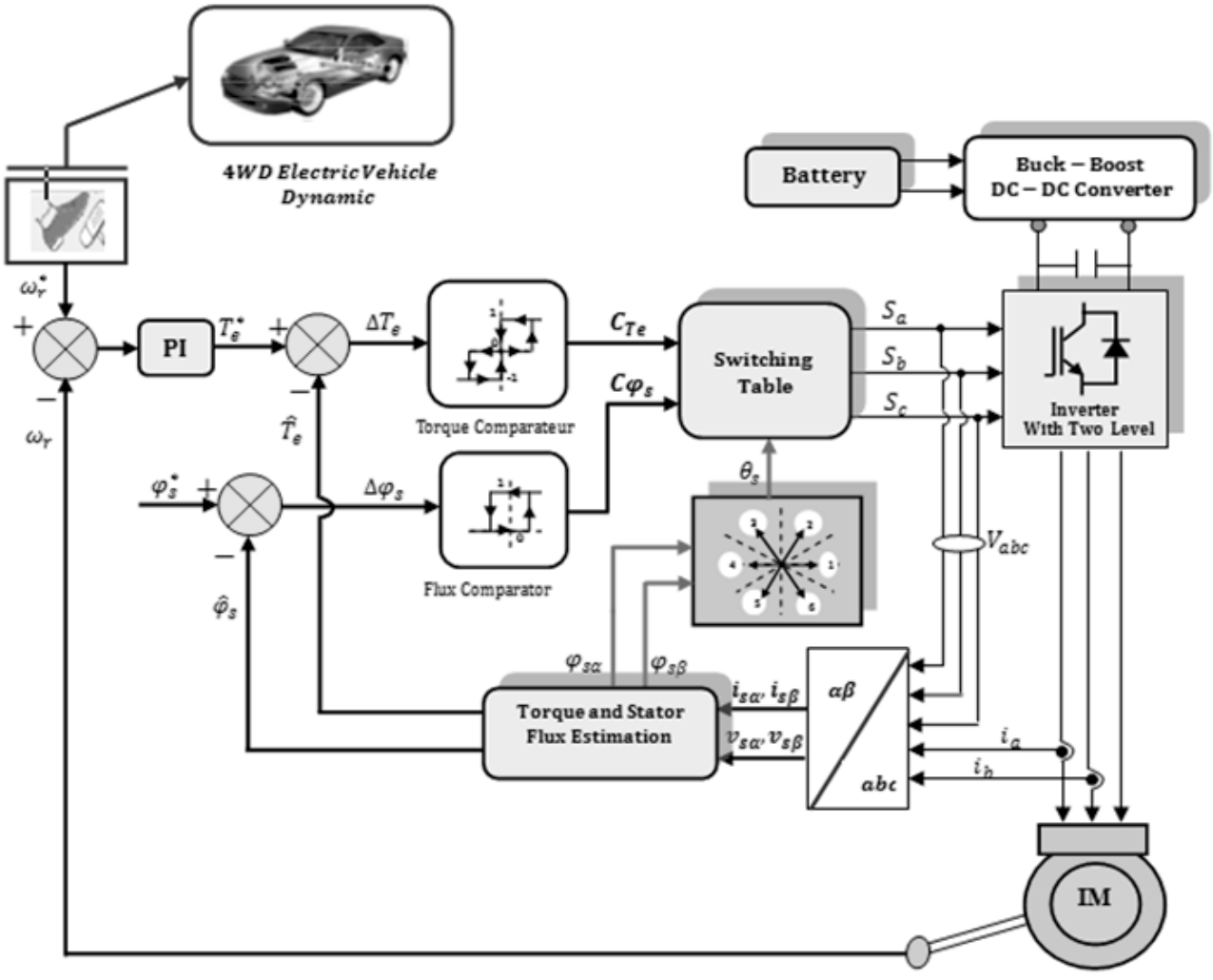

Fig. 2. Direct torque control DTC block diagram

converter) controlled by a PI type voltage regulator. The DC bus feeds the fourth induction motors through a voltage inverter (DC-AC converter). However, the drive motor shaft is coupled to the vehicle wheel via a power transmission line, each motor equipped with a fixed ratio gear and attached to the wheel constituting a driving wheel. This configuration is integrated in the wheels with fixed gear. The control method used for each in-wheel induction motor drive is the direct torque control (Fig. 2). The in-wheel motors are managed by an electronic differential. This system uses the position of the throttle and the angle of the steering wheel defined by the rotation of the wheel at the main position as inputs.

2.1. Traction Induction Motor Model

In This paper three-phase induction motors (IMs) are used. The induction motor model, with the stator currents and the stator flux as state variables, in the stationary (α, β) reference frame can be expressed by [10]:

$$\begin{cases} \dfrac{di_{s\alpha}}{dt} = -\eta i_{s\alpha} - \omega_r i_{s\beta} + K\varphi_{s\alpha} + \dfrac{1}{\sigma L_s}\omega_r \varphi_{s\beta} + \alpha V_{s\alpha} \\ \dfrac{di_{s\alpha}}{dt} = -\eta i_{s\beta} + \omega_r i_{s\alpha} + K\varphi_{s\beta} - \dfrac{1}{\sigma L_s}\omega_r \varphi_{s\beta} + \alpha V_{s\alpha} \\ \dfrac{d\varphi_{s\alpha}}{dt} = V_{s\alpha} - R_s i_{s\alpha} \\ \dfrac{d\varphi_{s\beta}}{dt} = V_{s\beta} - R_s i_{s\beta} \\ \dfrac{d\omega_r}{dt} = \dfrac{3p}{2J}(\varphi_{s\alpha} i_{s\beta} - \varphi_{s\beta} i_{s\alpha}) - \dfrac{B}{J}\omega_r - \dfrac{T_L}{J} \end{cases} \quad (1)$$

With

$$\eta = \left(\frac{R_s}{\sigma L_s} + \frac{R_r}{\sigma L_r}\right) \quad K = \frac{R_s}{\sigma L_s L_r} \quad \alpha = \frac{1}{\sigma L_s},$$

$$\sigma = 1 - \frac{M^2}{L_s L_r} \quad (2)$$

Where $u_{s\alpha}$, $u_{s\beta}$, $\varphi_{s\alpha}$, $\varphi_{s\beta}$, $i_{s\alpha}$, $i_{s\beta}$ are respectively the stator voltage, stator flux and stator current vector components in (α, β) stator coordinate system, ω_r is the rotor electrical angular, L_s, L_r, M are stator, rotor and magnetizing inductances respectively, R_s, R_r are respectively stator and rotor resistances, σ is the redefined leakage inductance, T_e and T_L is electromagnetic torque and load torque, J, B are the rotor inertia and fractional coefficient, p is the number of pairs poles.

2.2. Conventional Direct Torque Control Strategy for One in-Wheel IM

The conventional direct torque control strategy is developed in 1986 by Takahashi [7]. It is based on the direct determination of the control sequence applied to the switches of a voltage inverter. Fig. 2 shows the block diagram of the DTC technique. The measured speed of the motor is compared with the reference speed ω_r*, the error obtained is processed by a PI-type controller. The controller produces the reference torque value T_e*. The reference flux value φ_s* is determined from the parameters of the induction motor. The torque T_e, the stator flux φ_s and the flux angle θ_s of the induction motor are estimated using the measurements of the two stator phase currents and the DC-Link voltages (*Udc*). The estimated stator flux and the estimated torque are compared with their reference values φ_s* and T_e* respectively. The obtained errors are applied to the two levels hysteresis controller for flux control and three levels hysteresis controller for torque control. The outputs of the stator flux and torque hysteresis controllers, torque and the stator flux sector (where $C_{\varphi s}$ is the stator flux error after the hysteresis block, C_{Te} is the torque error after the hysteresis block and N_i (i = 1, ..., 6) means the sector) are the inputs of a switching table. This table generates the convenient combinations of the (ON or OFF) states of the inverter power switches. There are seven possible switching combinations, with two corresponding to the zero voltage space vectors which are (000) and (111). (6 active states V_1 to V_6 and 2 states zero V_0, V_7). When the stator flux is in sector N, if the torque and flux errors increase, if the torque error increases but the flux error decreases V_{N+2} are selected. The estimated value of flux and its phase angle is calculated in expression 3, 4, 5 and 6, respectively [11].

$$\begin{cases} \varphi_{s\alpha} = \int_0^t (V_{s\alpha} - R_s i_{s\alpha})dt \\ \varphi_{s\beta} = \int_0^t (V_{s\beta} - R_s i_{s\beta})dt \end{cases} \quad (3)$$

$$\varphi_s = \sqrt{\varphi_{s\alpha}^2 + \varphi_{s\beta}^2} \quad (4)$$

$$\theta_s = \operatorname{artg}\left(\frac{\varphi_{s\beta}}{\varphi_{s\alpha}}\right) \quad (5)$$

Where $\varphi_{s\alpha}$, $\varphi_{s\beta}$ are the α and β axes stator Flux, φ_s is the stator Flux, θ_s is the phase angle.

And the torque is controlled by three-level hysteresis. Its estimation value is calculated in expression (6).

$$T_e = \frac{3}{2}p\left(\varphi_{s\alpha} i_{s\beta} - \varphi_{s\beta} i_{s\alpha}\right) \quad (6)$$

3. 4WD Electric Vehicle Dynamic Modeling

3.1. Vehicle Dynamic

Based on the principals of vehicles mechanical and aerodynamics. The external forces acting on the vehicle in the longitudinal direction (Fig. 3) [12], [13], [14] are: the rolling resistance force F_{RR} due to friction of the vehicle tires on the road; the aerodynamic drag force F_{aero} caused by the friction on the body moving through the air, and the climbing force F_C, that depends on the road slope, the acceleration force F_{acc}.

The total tractive resistive force F_R of the 4WDEV is the sum of resistive force, as in (7) [14]

$$F_R = F_{RR} + F_{aero} + F_C + F_{acc} \quad (7)$$

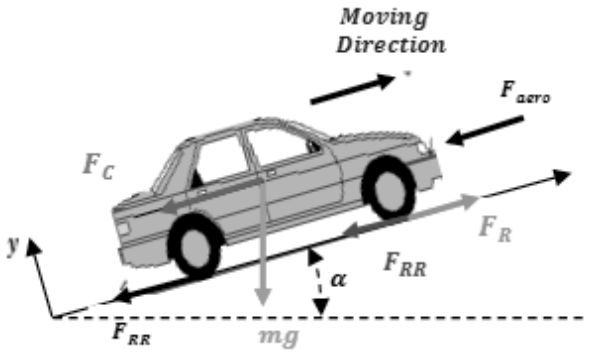

Fig. 3. Forces exerted on the 4WD electric vehicle

Where the force are given by:

1) The rolling resistance force (F_{RR}) is defined by:

$$F_{RR} = mgC_R \cos(\alpha) \tag{8}$$

2) The aerodynamic drag force (F_{aero}) is given by:

$$F_{aero} = \frac{1}{2}\rho_{air} A_f C_d V_{veh}^2 \tag{9}$$

3) The hill climbing force (F_C) is: the force on the vehicle to move up or move upward with a slope

$$F_C = \pm mg \sin(\alpha) \tag{10}$$

4) The force related to acceleration (F_{acc}) is:

$$F_{acc} = m\frac{dV_{veh}}{dt} = m\gamma \tag{11}$$

Finally the resisting couple F_R is given by

$$F_R = mgC_R \cos(\alpha) + \frac{1}{2}\rho_{air} A_f C_d V_{veh}^2 + mg \sin(\alpha) \tag{12}$$

The final expression of total resistive torque T_R is given by

$$\begin{aligned} T_R &= R_w F_R \\ &= mgC_R R_w \cos(\alpha) + \frac{1}{2}\rho_{air} A_f C_d R_w V_{veh}^2 \\ &\quad + mgR_w \sin(\alpha) \end{aligned} \tag{13}$$

Where m (kg) is the total mass of the vehicle, g (m/s²) is the acceleration of gravity; C_r is the tire rolling resistance coefficient and α (rad) is the road slope angle; ρ_{air} (kg/m³) is the mass density of air; A_f (m²) is the frontal area of the vehicle; C_d is the aerodynamic drag coefficient and V_{veh} (m) is the vehicle speed; R_w (m) is the wheel radius.

3.2. Dynamics of the Driving Wheel

The dynamics of each in-wheel motor drive system may be expressed as

$$J_{ij}\frac{d\omega_{r\_ij}}{dt} = T_{e-ij} - B_{ij}\omega_{r\_ij} - T_{R-ij} \quad \{ij\} = lf\ rf\ lr\ rr \tag{14}$$

J_{ij} and B_{ij} are the moment of inertia and friction coefficient of each motor, respectively and subscripts *lf, rf, lr* and *rr* mean left-front, right-front, left-rear and right-rear, respectively.

Where

$$T_{R-ij} = \frac{T_R}{2} = \frac{R_w}{2}F_R \tag{15}$$

Thin the speed of each in-wheel is given by

$$\begin{cases} \dot{\omega}_{r\_lf} = \dfrac{1}{J_{lf}}\left(T_{e-lf} - B_{lf}\omega_{r\_lf} - T_{R\_lf}\right) \\ \dot{\omega}_{r\_rf} = \dfrac{1}{J_{rf}}\left(T_{e-rf} - B_{rf}\omega_{r\_rf} - T_{R\_rf}\right) \\ \dot{\omega}_{r\_lr} = \dfrac{1}{J_{lr}}\left(T_{e-lr} - B_{lr}\omega_{r\_lr} - T_{R\_lr}\right) \\ \dot{\omega}_{r\_rr} = \dfrac{1}{J_{rr}}\left(T_{e-rr} - B_{rr}\omega_{r\_rr} - T_{R\_rr}\right) \end{cases} \tag{16}$$

Each motor is equipped with a fixed ratio speed reducer and attached to the wheel constituting a driving wheel [15]. The gear is modelled by the gear ratio, the transmission efficiency and its inertia, i.e.

$$\begin{cases} \omega_{wheel-ij} = \dfrac{\omega_{r-ij}}{k_{gear}} \\ T_{wheel-ij} = T_{e-ij} k_{gear} \eta_t \end{cases} \tag{17}$$

Where η_t efficiency of the gearbox; *kgear* is the gearbox coefficient.

The total moment of inertia associated with the vehicle (J_{ij}), in the motor referential is given by

$$\begin{cases} J_{ij} = J_{wheel} + J_V + J_{m-ij} \\ J_V = \dfrac{1}{2}m\left(\dfrac{R_w}{k_{gear}}\right)^2(1-\lambda) \end{cases} \tag{18}$$

Where J_{wheel} wheel is the shaft inertia moment including the motor and wheel inertia, J_v is the inertia moment of the vehicle, λ represent the slipping of the wheel (λ is usually low and can be neglected if the adhesion coefficient of the road is high).

3.3. Modeling of Electronic Differential System (EDS)

The EDS for Electric vehicle with four independent in-wheels motors is a very complex control system, it needs the control for different speeds simultaneously. Fig. 4(a) is presented the proposed electronic differential structure, where the left and right front wheels, the left and right rear wheels are controlled by using four in-wheel motors. The Induction motors are preferred due to the high-efficiency, high torque density, silent operation and the low maintenance favours of the electric vehicle applica-

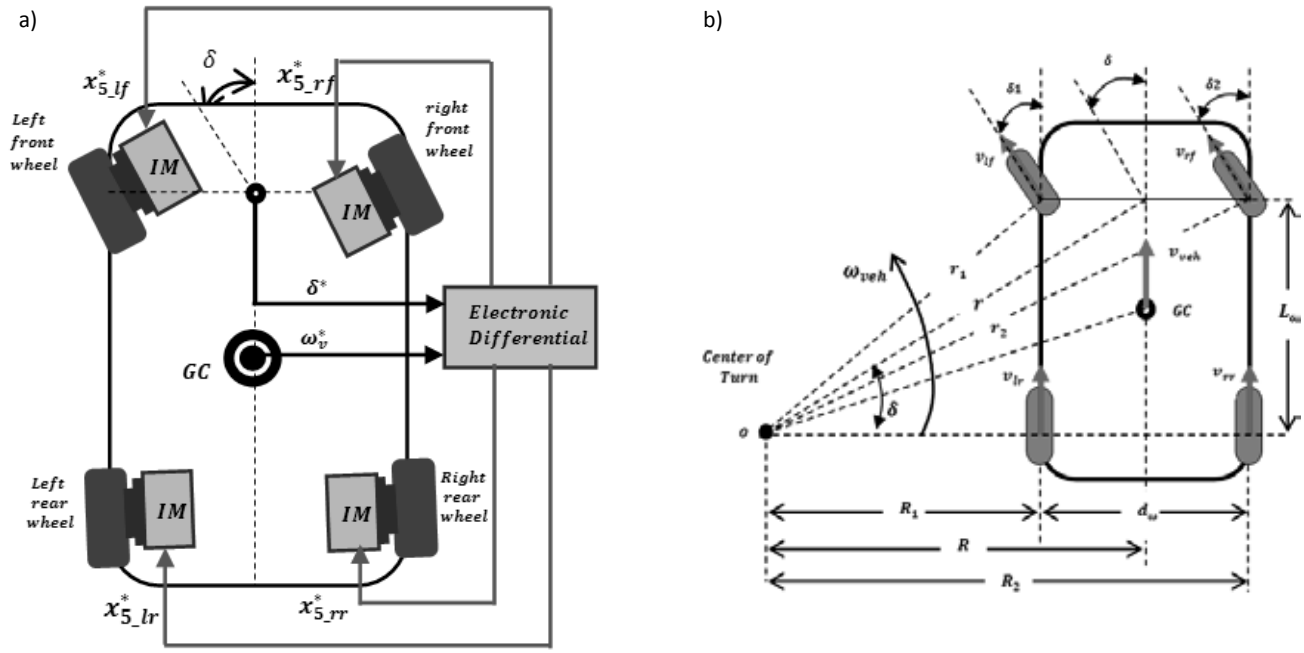

Fig. 4. (a) Proposed Electronic Differential, (b) Kinematic Model of the 4WDEV driven during a curve

tion. Two inputs steering angle and throttle position collectively are decided the speeds of the right and left wheel (front and rear) to prevent the vehicle from slipping. For a right turn, the differential has to keep up a higher speed at the left front and left rear wheels than the right front and right rear wheels to prevent the tires from losing traction while turning. The Ackerman and Jeanted [14] shown Fig. 4(b) can be used. It shows the kinematic model of the proposed system in a left turning manoeuvre. The relevant parameters are shown in Table 1.

Table 1.Definition of parameters in kinematic model

Elements	Name
ω_{veh}	Reference speed of vehicle.
δ	Steering Angle (°)
δ_1	Turning angle of left front wheel, (°)
δ_2	Turning angle of right front wheel, (°)
L_ω	Length of vehicle, (m)
d_ω	Width of vehicle, (m)
R	Steering radius of center of rear axle
R_1	Steering radius of inside rear wheel.
R_2	Steering radius of outside rear wheel.
r	Steering radius of center of front axle.
r_1	Steering radius of inside front wheel.
r_2	Steering radius of outside front wheel.
v_{lf}, v_{rf}	Linear speed of left front in-wheel and right front in-wheel
v_{lr}, v_{rr}	Linear speed of left rear in-wheel and right rear in-wheel.

From this model, the following characters can be calculated

$$\begin{cases} R = \dfrac{L_w}{\tan(\delta)} \\ R_1 = R - \dfrac{d_w}{2} \\ R_2 = R + \dfrac{d_w}{2} \end{cases} \tag{19}$$

The steering radius of two front in-wheels motor drive can also be calculated by the geometrical relationship

$$\begin{cases} r = \sqrt{L_w^2 + R^2} \\ r_1 = \sqrt{L_w^2 + R_1^2} = \sqrt{L_w^2 + \left(R - \dfrac{d_w}{2}\right)^2} \\ r_2 = \sqrt{L_w^2 + R_2^2} = \sqrt{L_w^2 + \left(R + \dfrac{d_w}{2}\right)^2} \end{cases} \tag{20}$$

By applying the instantaneous center theorem. The angular velocity speeds of the two fronts and rear in-wheels motor drive are given by

$$\begin{cases} \omega_{lf} = \omega_{veh} \dfrac{\sqrt{1+\left(\cot(\delta)-\dfrac{d_w}{2L_w}\right)^2}}{\sqrt{1+\left(\cot(\delta)\right)^2}} \\ \omega_{rf} = \omega_{veh} \dfrac{\sqrt{1+\left(\cot(\delta)+\dfrac{d_w}{2L_w}\right)^2}}{\sqrt{1+\left(\cot(\delta)\right)^2}} \\ \omega_{lr} = \omega_{veh}\left(1-\dfrac{d_w \tan(\delta)}{2L_w}\right) \\ \omega_{rr} = \omega_{veh}\left(1+\dfrac{d_w \tan(\delta)}{2L_w}\right) \end{cases} \quad (21)$$

According to equation (20) and equation (21), the speed reference of four in-wheels induction motors are expressed as

$$\begin{cases} \omega^*_{r\_lf} = k_{gear}\omega^*_{lf} = k_{gear}\omega^*_{veh} \dfrac{\sqrt{1+\left(\cot(\delta)-\dfrac{d_w}{2L_w}\right)^2}}{\sqrt{1+\left(\cot(\delta)\right)^2}} \\ \omega^*_{r\_rf} = k_{gear}\omega^*_{rf} = k_{gear}\omega^*_{veh} \dfrac{\sqrt{1+\left(\cot(\delta)+\dfrac{d_w}{2L_w}\right)^2}}{\sqrt{1+\left(\cot(\delta)\right)^2}} \\ \omega^*_{r\_lr} = k_{gear}\omega^*_{lr} = k_{gear}\omega^*_{veh}\left(1-\dfrac{d_w \tan(\delta)}{2L_w}\right) \\ \omega^*_{r\_rr} = k_{gear}\omega^*_{lrr} = k_{gear}\omega^*_{veh}(1+\dfrac{d_w \tan(\delta)}{2L_w}) \end{cases} \quad (22)$$

Where k_{gear} is the gearbox ratio, ω^*_{veh} is the angular reference speed of the vehicle and ω^*_{lf}, ω^*_{rf}, ω^*_{lr}, ω^*_{rr} are the speed references of left front wheel, right front wheel, left rear wheel and right rear wheel respectively.

3.4. Synthesis of the Different Speed Controllers of One in-Wheel IM

The synthesis of a command must be allowed by the calculation of the instructions to be applied to the actuators so that the vehicle can perform a specified movement. A number of different type's controller for speed control of an induction motor for this electric vehicle application that has been investigated. PI (proportional and integral) and Fuzzy Logic controllers were chosen for simulation. The structure of the speed control is shown as the external loop in Fig. 5. The steering angle δ and reference angular speed of the vehicle ω^*_{veh} are fed to Electronic Differential (ED). The ED algorithm produces the speed reference of the front and rear in-wheel motor ($\omega^*_{r\_lf}$, $\omega^*_{r\_rf}$, $\omega^*_{r\_lr}$, $\omega^*_{r\_rr}$). The reference and actual speed of each in-wheels motor are the inputs of the speed controller blocks. The speed error is used in PI and Fuzzy Logic speed controllers. The closed-loop speed controller generates the reference motor torque $T^*_{e\_ij}$.

3.4.1. PI Speed Controller Design

If we want the effect of external disturbances to be zero and if the speed is constant. And assume all the initial conditions are zero. The Laplace transfer function of (14) can be given as:

$$G(s) \approx \frac{\omega_{r\_ij}(s)}{T_{e-ij}(s)} = \frac{1}{J_{ij}s + B_{ij}} \quad (23)$$

Therefore, the closed PI controller loop is

$$F(s) = \frac{k_p s + k_I}{J_{ij}s^2 + (k_p + B_{ij})s + k_I} \quad (24)$$

The denominator in equations (24) can be rewritten as

$$s^2 + \frac{(k_p + B_{ij})}{J_{ij}}s + \frac{k_I}{J_{ij}} \quad (25)$$

So resonance frequency ω_n and damping ratio ξ are given by

$$\omega_n = \sqrt{\frac{k_I}{J_{ij}}} \;\; \xi = \frac{k_p + B_{ij}}{2\sqrt{k_I J_{ij}}} \quad (26)$$

Therefore, k_p and k_i can be determined as:

$$\begin{cases} k_p = 2\xi\omega_n J_{ij} - B_{ij} \\ k_I = \omega_n^2 J_{ij} \end{cases} \quad (27)$$

To optimize dynamic performance and system stability, we opt for a closed-loop damping coefficient ξ of value equal to 0.7.

The law of PI controller for the four in-wheel induction motors is:

$$T^*_{e\_ij} = k_p\left(\omega^*_{r\_ij} - \omega_{r\_ij}\right) + k_I \int_0^t \left(\omega^*_{r\_ij} - \omega_{r\_ij}\right)dt \quad (28)$$

3.4.2. Fuzzy Logic Speed Controller Design (FLC)

In this section, the PI speed controller is replaced by the fuzzy logic controller (FLC). The schematic model of the proposed FLC is shown in Fig. 6. It can be seen that direct torque control (DTC) method is employed in the given block diagram. The proposed control system (as shown in Fig. 2) has two inputs: the first is the desired speed of the motor ($\omega^*_{r\_ij}$). The second input is the feedback signal, which represents the actual motor speed (ω_{r_ij}). FLC was applied to this system to control the speed of the induction motor.

Similar to PI speed controller, the speed error signal (e) is fed into FLC to determine the measured rotor speed (ω_{r_ij}). The inputs variables of FLC are speed error (e) (i.e. equation 29) and rate of change in speed error (Δe) (i.e. equation 29) and the output variable is

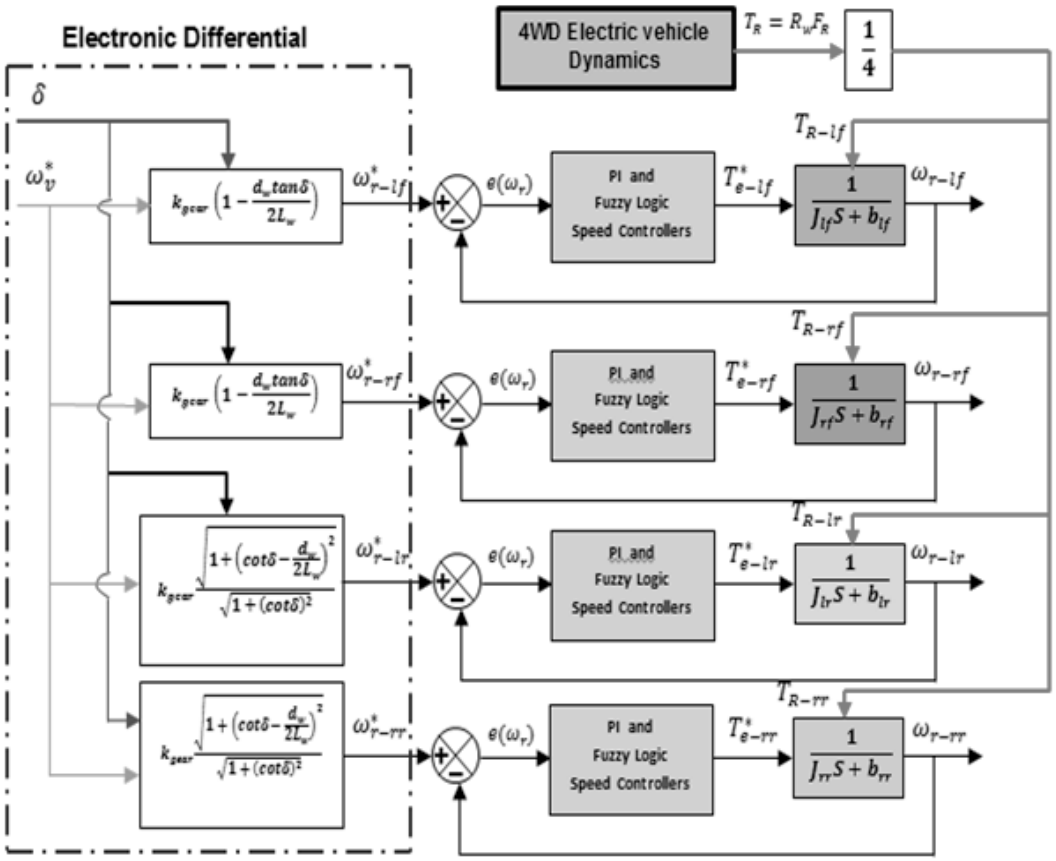

Fig. 5. General configuration of the four in-wheel motor drives speed control strategy

the reference torque value ($T^*_{e\_ij}$) for the DTC which is shown in Fig. 7 and Fig. 8.

$$\begin{cases} e = \omega^*_{r\_ij} - \omega_{r\_ij} \\ \Delta e = e(k) - e(k-1) \end{cases} \tag{29}$$

Where indices (*k*) and (*k-1*) indicate the present state and the previous state of the system, respectively.

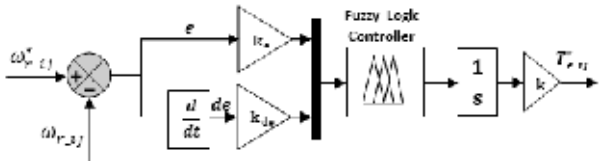

Fig. 6. Block diagram of the proposed fuzzy logic speed control system with DTC

In this control scheme, the Mamdani type, triangular membership function MFs (i.e. 7MFs) for the input and output variables, the max-min reasoning method, and the centroid method for the defuzzification are used [16]. The triangular-shaped membership functions for input *(e* and *Δe*) and output ($T^*_{e\_ij}$) variables are shown in Fig. 7 and Fig. 8, respectively. The proposed fuzzy sets (linguistic definition) and MFs for inputs and output variables are defined as follows: GN (Grand Negative), MN (Medium Negative), PN (Small Negative), ZE (Zero Error), PP (Small Positive), MP (Medium Positive), GP (Big Positive). Seven membership functions (MFs) are chosen for the inputs (*e* and *Δe*) and seven for the output ($T^*_{e\_ij}$) variable. All the MFs are normalized to be between [–1, 1].

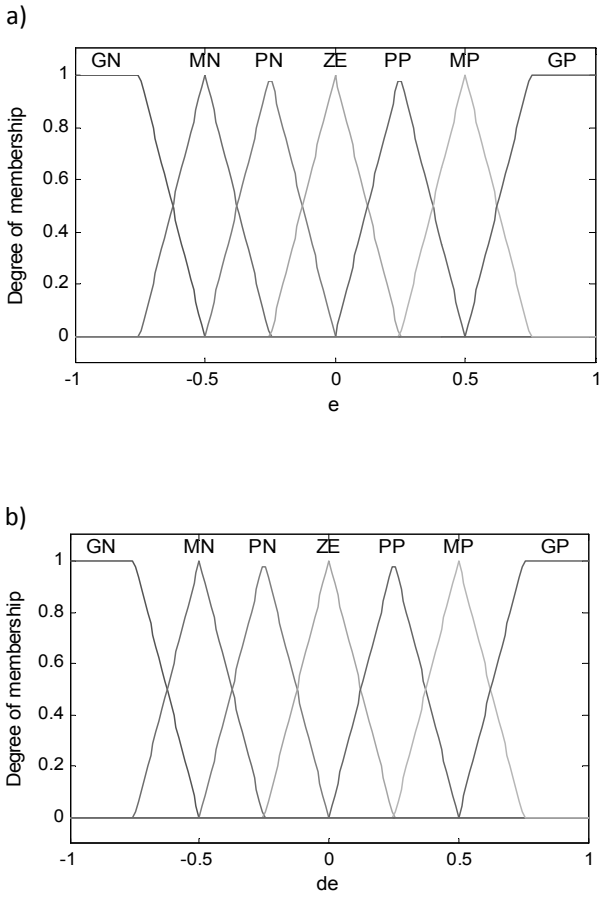

Fig. 7. Membership functions for the (a) inputs error (e) and (b) change in Error (Δe)

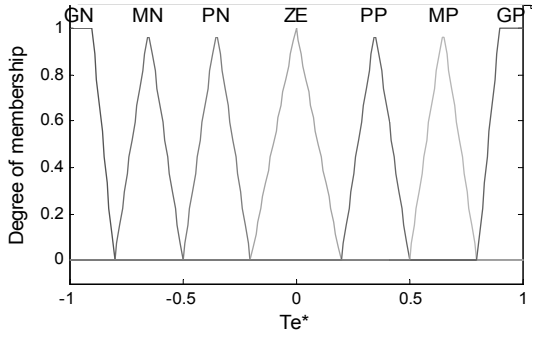

Fig. 8. Membership functions for the output change of control ($T^*_{e\_ij}$)

The total number of possible linguistic rules used in the proposed fuzzy logic speed controller contains forty-nine (49) rules for each output. The resulting fuzzy inference rules for the output variable $T^*_{e\_ij}$ are shown in Table 2.

Table 2. Fuzzy tuning rules

		e						
		GN	**MN**	**PN**	**ZE**	**PP**	**MP**	**GP**
Δe	**GN**	GN	GN	MN	MN	PN	PN	ZE
	MN	GN	MN	MN	PN	PN	ZE	PP
	PN	MN	MN	PN	PN	ZE	PP	PP
	ZE	MN	PN	PN	ZE	PP	PP	MP
	PP	PN	PN	ZE	PP	PP	MP	MP
	MP	PN	ZE	PP	PP	MP	MP	GP
	GP	ZE	PP	PP	MP	MP	GP	GN

The rules the of fuzzy logic system can be explained using examples:

- If (speed error is MN) and (change in speed error is GN), then (reference torque variation is GN).
- If (speed error is GN) and (change in speed error is GN), then (reference torque variation is GN).

The fuzzy rules and surface viewer of the proposed controller are shown in Fig. 9.

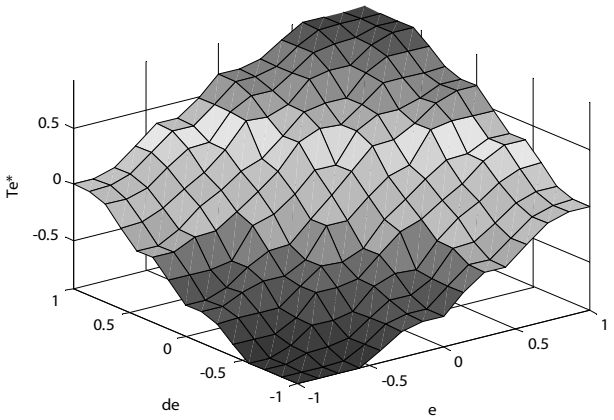

Fig. 9. Three dimensional plot of the control surface

3.5. Vehicle Reference Speed Profile

Before calculating the reference torque has been made of each motor wheel, it is necessary to define a speed profile that faithfully represents the movements that the vehicle will have to perform. The specified road trajectory is shown in Fig. 10. This trajectory is defined by three phases successively. In the first one the vehicle is moving on the curved road at right side with speed of 50 km/h, the second phase present the acceleration phase's beginning with 80Km/h in curved road at left side, and finally the vehicle is moving up the slopped (climbing) road of 10% under 30 km/h, the speed road constraints are described in Table 3.

Table 3. Specified driving route topology

Phase	**Time (Sec)**	**Event information**	**Vehicle speed km/h**
01	0s < *t* < 4s	curved road at right side	50 km/h
02	4s < *t* < 7.5s	Acceleration and curved road	80 km/h
03	7.5s < *t* < 10s	Climbing a slope 10%	30 km/h

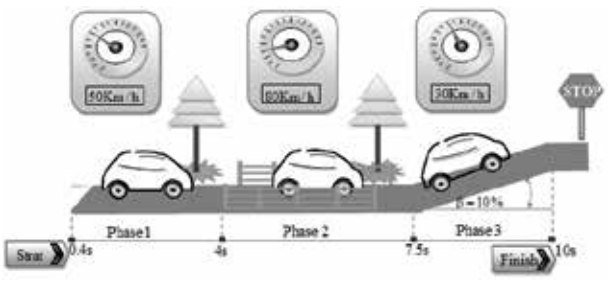

Fig. 10. Specify driving road topology

4. Simulation Results

To check and compare the effectiveness of the different speed controllers (PI and FLC) proposed in this study. In this section, numerical simulations were preformed using Matlab / Simulink environment, on the traction system by an electric vehicle propelled by four different 15 Kw induction motors integrated in the front and rear wheels (4WDEV) see the model in Fig. 2. The aims of the simulation carried out evaluated the efficiency of the different speed controllers (classical PI and FLC proposed) on the dynamics of the electrical vehicle, a comparison of which was made between the two. This system has been simulated by a reference vehicle speed given by the topology illustrated in Fig. 10. Table 4 summarizes the mechanical and aerodynamic characteristics of 4WD electric vehicles. The induction motor parameters are given in Table 5.

In order to ensure and confirm the effectiveness of the DTC control strategy on the traction system by 4WDEV. The system has been subjected to a change in the reference speed according to the topology shown in Fig. 10. At this stage of operation two turns are imposed by the driver on the vehicle chassis by steering angle, one to the right (phase 01) at time t = 1.7 sec and the other at left t = 5.5 sec.

Table 4. Proposed 4WD electric vehicle parameters

Parameters Name	Value
Wheel radius, R_w (m)	0.32
Vehicle mass, m (kg)	1300
Aerodynamic drag coefficient, C_d	0.3
Vehicle frontal area, A_f (m^2)	2.60
Tire rolling resistance coefficient, C_r	0.01
Air density, ρ_{air} (kg/ m^2)	1.2
Gear coefficient, k_{gear}	5
Width of vehicle, d_ω (m)	1.5
Length of vehicle, L_ω (m)	2.5

Table 5. Induction motor parameters

Parameters Name	Value
Rotor Inductance, L_r (H)	0.0651
Rotor Inductance, L_s (H)	0.0651
Mutual Inductance, M (H)	0.06419
Stator Resistance, R_s (Ohm)	0.2147
Rotor Resistance, R_r (Ohm)	0.2205
Number of pole pairs, p	2
Motor- load inertia, J ($Kg \cdot m^2$)	0.102
Rated power, J (Kw)	15
Viscous friction coefficient, J ($N \cdot m \cdot s$)	0.009541

Fig. 11 shows the curve of the steering angle of the front wheels given by the driver. The positive value corresponds to a right turn ($\delta = 20°$), and the negative value corresponds to a left turn ($\delta = -8°$).

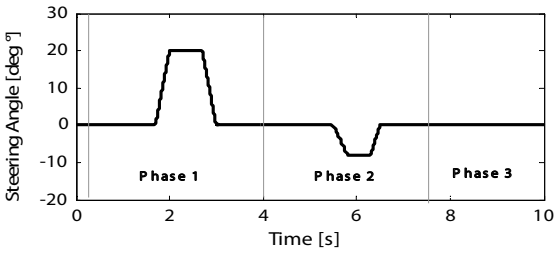

Fig. 11. Steering angle variation

The linear speeds of the front and rear wheels with PI and Fuzzy Logic controllers are shown in Fig. 12 (a) and (b), respectively. We assume that the turns are made at a constant speed, the driver gives a steering angle δ^* which begins to be a steering angle of the front wheels.

The electronic differential immediately acts on the fourth in-wheels IMs, decreasing the speed of the two wheels that are located inside the turn, and increasing the speed of the wheels located outside the turn. During the first pilot (phase 01), the two left front and rear wheels located outside the curved right turn are rotated at higher speeds than the two right side wheels (front and rear). On the other hand, it can be seen that the two front right and left rear wheels rotate at higher speeds than the two left side wheels during the second turn (phase 02) as shown in Fig. 12.

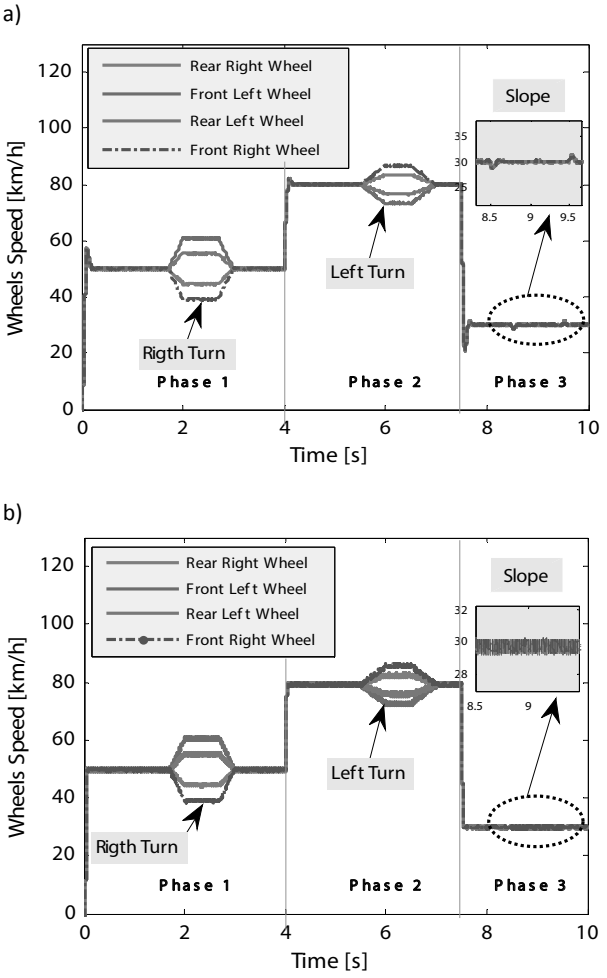

Fig. 12. Four wheels speed variation in different phases (a) PI, and (b) FLC

The comparative study of the speed response (Fig. 13 (a)) shows that the different controllers namely the classical PI and FLC, giving almost the same speed profile, but with a better rise time (convergence of actual speed to reference speed with minimum rise time), and zero Overshoot with zero static error in Fuzzy Logic controller, compared to the PI controller which present an overshoot equal 7.3980% and a rise time quite important. The effects of disturbances that appear clearly in the classical PI controller (where the vehicle is in a slope road phase 3). Table 6 shows the static and dynamic characteristics of all controllers.

Table 6. Performances of the PI and FLC in the speed response

Controller	Rise Time (sec)	Settling Time (sec)	Overshoot value	Peak Time (sec)
PI	0.2157	0.3235	7.3980	0.3340
FLC	0.1153	0.1918	0.0023	0.5260

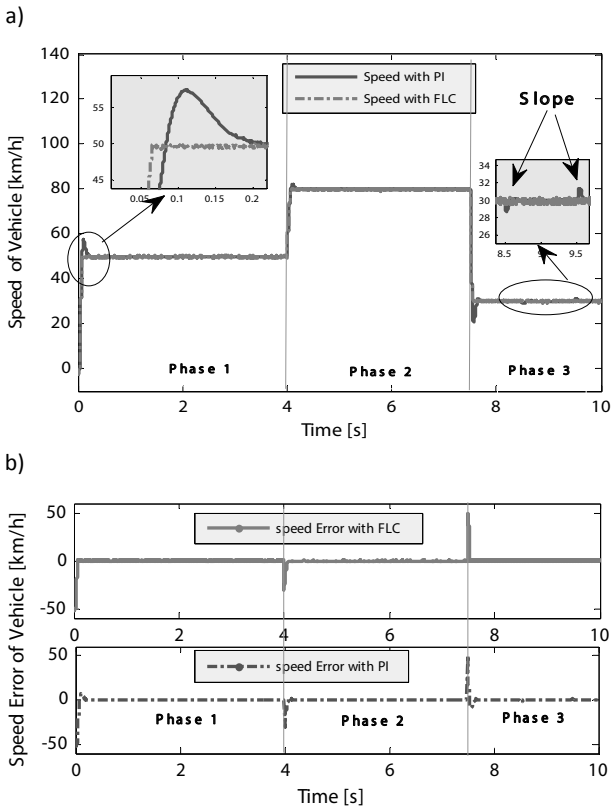

Fig. 13. Vehicle Linear speed (a) and error speed (b) variation in different phases using PI and FLC controllers

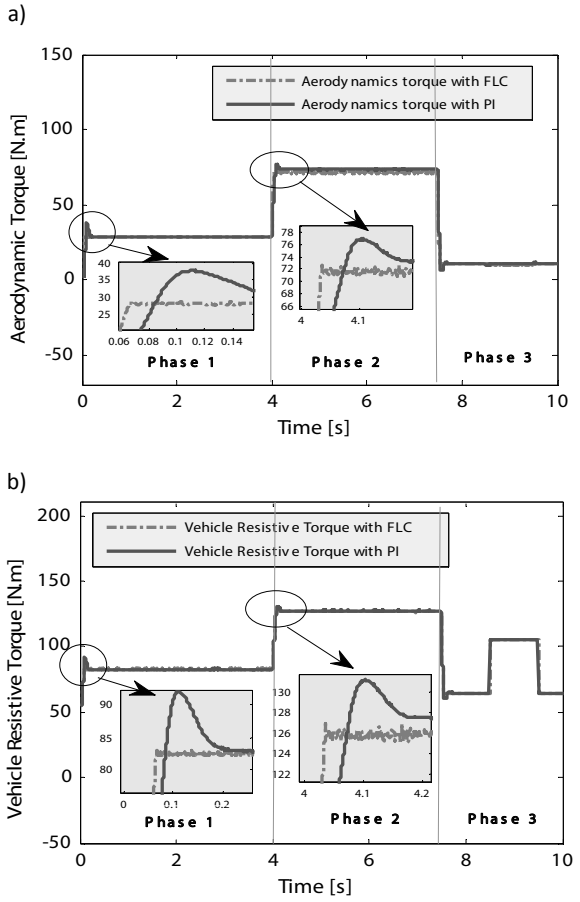

Fig. 14. Aerodynamic torque (a) and vehicle resistive torque (b) variation in different phases using PI and FLC controllers

Aerodynamic torque is reduced with Fuzzy Logic control relatively with PI. 73.42 Nm with FLC and 72.11 Nm by PI (phase 2, see Figure 14 (a)). This value can be explained because of the large frontal area in the case of PI versus FLC. It can be seen that the overall resistive torque is improved in the FLC compared to the PI (See Figure 14 (b)). Table 7 summarizes this improvement.

Table 7. Values of the vehicle resistive torque and aerodynamic torque in different phases

Phase	Aerodynamics Torque (T_{aero})		Vehicle resistive Torque (T_R)	
	PI	FLC	PI	FLC
01	28.21	28.62	82.91	82.63
02	73.42	72.11	127.68	127.42
03	10.32	10.16	64.54	64.51

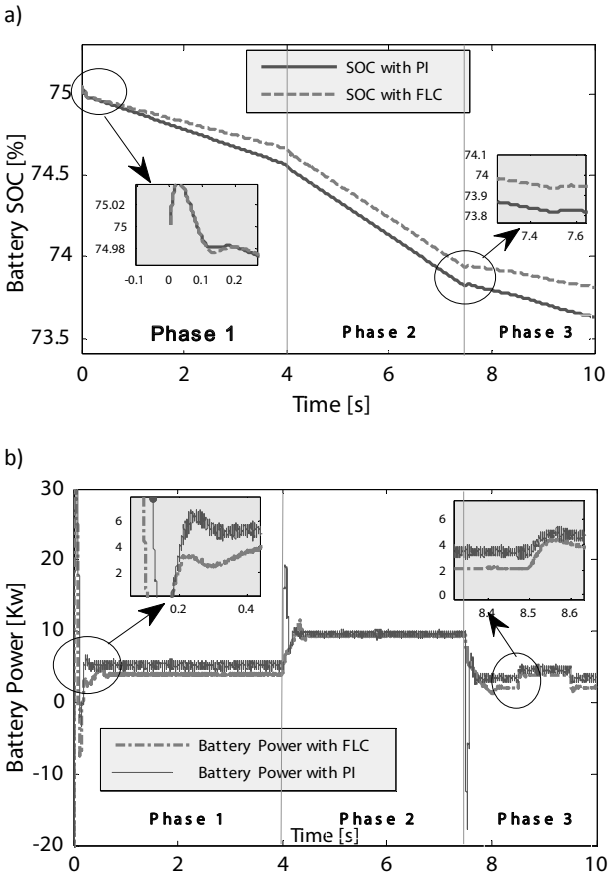

Fig. 15. State of charge SOC (a) and Power Battery (b) variation in different phase using PI and FLC controllers

Figure 15 (a) and (b) explain the variation of the state of charge and the power of the battery respectively of this driving cycle. Figure 15 (a) shows how the SOC in the lithium-ion battery (battery initialized to 75% at the start of the simulation). The latter varies with the driving cycle for control methods. The state of charge of the battery decreases rapidly at acceleration and on a slope. Energy consumption is low at Fuzzy logic speed controller relatively with PI. The SOC variation is between 75% and 73.83% (difference of 1.17%). Table 8 shows the variation

of SOC during the driving cycle. Figure 15 (b) shows the variation of battery power in different phases of travel where it can be seen that the battery provides approximately 5.24 Kw (PI controller) and 3.92 Kw (Fuzzy Logic controller) to achieve the desired speed in the first phase. The power is the same during phase 2 equal to 9.87 Kw with PI and 9.35 Kw with FLC. The power delivered (Figure 15 (b)) increases when in the slope of 10° (phase 3) is equal to 4.60 Kw by PI and 2.11 Kw with FLC. As a comparison, the Fuzzy Logic speed controller strategy reduces energy consumption compared to the PI. Figure 16 and Table 9 shows that the crossed distance by the vehicle is improved by the Fuzzy Logic speed controller compared to classical PI (541.84 m with PI and 552.66 m in FLC). Autonomy is increased by 10.82 m by the Fuzzy Logic speed controller.

Table 8. Evaluation of Li-Ion battery SOC in different phases

Phase	Begin Phase [sec]	End Phase [sec]	SOC [%] with PI	SOC [%] with FLC
01	0	4	74.57	74.67
02	4	7.5	73.82	73.93
03	7.5	10	73.64	73.83

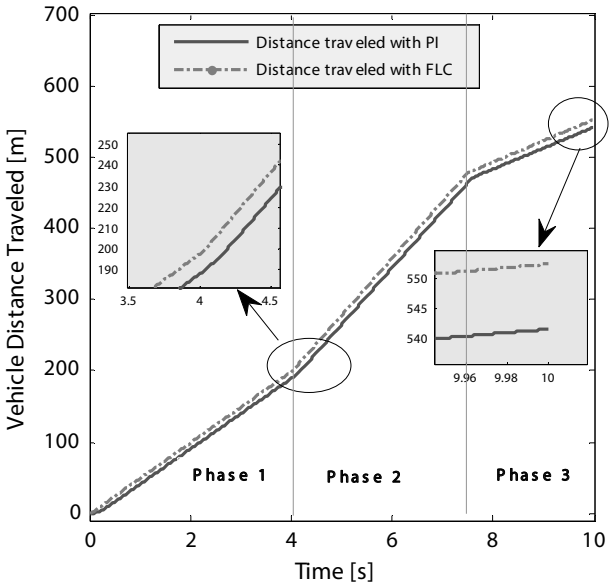

Fig. 16. The vehicle travelled distance in the different phase using PI and FLC controllers

Table 9. Variation of battery power and distance travelled in different trajectory phases

Phase	Battery Power Consumed [Kw]		Vehicle Driven Distance [m]	
	PI	FLC	PI	FLC
1	5.24	3.92	188.21	197.52
2	9.87	9.35	274.31	280.02
3	3.50	2.11	79.32	75.12

5. Conclusions

The research proposed in this paper has demonstrated the possibility of an improved four wheels vehicle stability which utilize four independent driving in-wheels for motion by using the Fuzzy Logic controller.

The study of four wheels independent wheel control approach structure applied to the electric chain system using the intelligent speed control which ensure the driving on slope with high safety conditions.

The results obtained by Matlab simulation proves that this structure permits the realization of Fuzzy Logic loop speed control which gives a good dynamic performances of electric vehicle. The proposed control, permits to control independently the driving in-wheels speeds with high accuracy in flat roads or curved ones in each case. The slope's road does no. affect the performances of the driving motor wheels stability comparing with the PI classical controller.

ACKNOWLEDGEMENT

This work was supported by the Laboratory of Smart Grids & Renewable Energies (S.G.R.E).Faculty of Technology, Department of Electrical Engineering, and Bechar University, Algeria.

AUTHORS

Abdelkader Ghezouani*, Brahim Gasbaoui, Nourai Nair and Othmane Abdelkhalek – Faculty of Sciences and Technology, Department of Electrical Engineering Bechar. University B.P 417 Bechar (08000), Algeria.

Jemal Ghouili – Department of Electrical Engineering, Moncton University (Canada).

*Corresponding author

REFERENCES

[1] Kim J., Jung J., and Nam K., "Dual-inverter control strategy for high-speed operation of EV induction motors", *IEEE Trans. Ind. Electronics,* 2004, vol. 51, no. 1, pp. 312–320. DOI: 10.1109/TIE.2004.825232.

[2] Gregory A. H., Kamal Y. T., "Modeling and simulation of a hybrid-electric vehicle drive train". In: *Proceedings of the American Control Conference*, 1997, pp. 636–640.

[3] Baba A., "Optimisation du flux dans la machine à induction par une commande vectorielle: minimisation des pertes", *Thèse de Doctorat en Génie Electrique Pierre & Marie Curie Paris*, 5–7 Janvier, 1997 (in French).

[4] Triqui N., "Motorisation Asynchrone pour Véhicule Electrique," *Institut Polytechnique de Lorraine Nancy Paris,* 1997 (in French).

[5] Casadei D., Profumo F., and Tani A., "FOC and DTC: Two viable schemes for induction motor torque control," *IEEE Trans of Power Electron-*

ics (S0885 – 993), 2002, vol. 17, pp. 779–787.

[6] Buja G. S., Kaźmierkowski M. P., "Direct Torque Control of PWM Inverter Fed. AC Motors–A survey," *IEEE Trans Power Electronics*, vol. 51, 2004.
DOI: 10.1109/TIE.2004.831717.

[7] Takahachi I., Noguchi T., "A New Quick-response and High Efficiency Control Strategy of an Induction Motor" , *IEEE Transaction on Industrial Applications,* 1986, vol. 5, pp. 820–827.

[8] Depenbrock M., "Direct self-control of inverter-fed machine", *IEEE Trans. Power Electron,* 1988, vol. 3, pp. 420–429.

[9] Heath H., Seth S. R., "Speed-Sensorless Vector Torque Control of Induction Machines Using a Two-Time-Scale Approach" , *IEEE Transactions on Industry Applications*, 1998 January--February, vol. 34, no. 1.

[10] Kaźmierkowski M.P., "Control Strategies for PWM Rectifier/Inverter-Fed Induction Motors", *Industrial Electronics ISIE Proceedings of the 2000 International Symposium IEEE*, 2000, vol. 1, pp. TU15-TU23.

[11] Ghezouani A., Gasbaoui B., Ghouili J., Benayed A. A., "An Efficiency No Adaptive Backstepping Speed Controller Based Direct Torque Control", *Journal of Automation, Mobile robotics & Intelligent Systems*, 2017, vol. 11, no. 1, pp. 56–63.
DOI: 10.14313/JAMRIS_1-2017/8.

[12] Husain I., et al., "Design, modeling and simulation of an electric vehicle system", *SAE Technical Paper Series*, 1999, pp. 01–1149.

[13] Ehsani M., et al., "Propulsion system design of electric and hybrid vehicle", *IEEE Trans. Ind. Electron*, 1997, vol.45, pp. 19–27.

[14] Gillespice T., "Fundamentals of vehicle dynamics", *Society of Automotive Engineers*, ISBN 1-56091-199-9.

[15] Hori.Y., "Future Vehicle Driven by Electricity and Control – Research on Four-Wheel-Motored UOT Electric March II," *IEEE Transactions on Industrial Electronics,* 2004, vol. 51, pp. 954–962.

[16] Aissaoui H., Abid M., Tahour A., and Zeblah A., "A Fuzzy Logic Controller for Synchronous Machine," *Journal of Electrical Engineering,* 2007, vol. 58, no. 5, pp. 285–290.